How Does Intracellular Ca^{2+} Oscillate: By Chance or by the Clock?

Alexander Skupin,* Helmut Kettenmann,† Ulrike Winkler,† Maria Wartenberg,‡ Heinrich Sauer,¶ Stephen C. Tovey,§ Colin W. Taylor,§ and Martin Falcke*

*Department of Theoretical Physics, Hahn Meitner Institut, Berlin, Germany; †Department of Cellular Neurosciences, Max Delbrück Center for Molecular Medicine, Berlin, Germany; ‡FZ Lobeda Kardiologie, Universitätsklinikum Jena, Jena, Germany; ¶Physiologisches Institut, Justus-Liebig-Universität, Giessen, Germany; and §Department of Pharmacology, University of Cambridge, Cambridge, United Kingdom

ABSTRACT Ca^{2+} oscillations have been considered to obey deterministic dynamics for almost two decades. We show for four cell types that Ca^{2+} oscillations are instead a sequence of random spikes. The standard deviation of the interspike intervals (ISIs) of individual spike trains is similar to the average ISI; it increases approximately linearly with the average ISI; and consecutive ISIs are uncorrelated. Decreasing the effective diffusion coefficient of free Ca^{2+} using Ca^{2+} buffers increases the average ISI and the standard deviation in agreement with the idea that individual spikes are caused by random wave nucleation. Array-enhanced coherence resonance leads to regular Ca^{2+} oscillations with small standard deviation of ISIs.

INTRODUCTION

How are random molecular events orchestrated into reliable cellular behavior like global intracellular Ca^{2+} oscillations? If many molecules are involved, it is generally assumed that the cell behaves like a continuously stirred reactor and the law of large numbers establishes predictable behavior (1). Most models of the dynamics of intracellular Ca^{2+} release adopt this idea (2–4), but it is not consistent with experimental analyses showing that global oscillations arise from Ca^{2+} waves initiated locally (5–9). Such a local mechanism is predicted to lead to stochastic oscillations because although each cell has many IP_3Rs and Ca^{2+} ions, the law of large numbers does not apply to the initiating event (3,10), which is restricted to very few IP_3Rs by steep Ca^{2+} concentration gradients (7,9,11). Indeed, the law of large numbers may not apply either to other signaling pathways that generate steep intracellular concentration gradients (12).

Oscillations of intracellular Ca^{2+} dynamics exhibit spike trains which appear rather regular by casual inspection. This led to formulation of models with an oscillatory deterministic regime (2–4), but cells might exhibit stochastic dynamics which produce very similar global signals. That type of dynamics, often described as a stochastic medium (10,13–16), was predicted theoretically for reaction-diffusion systems with discrete stochastic sources of the diffusing species. Intracellular Ca^{2+} dynamics may be perceived as a stochastic medium: the diffusing species is cytosolic Ca^{2+} and the discrete stochastic sources are ion channels. Such systems generate spatiotemporal structures by wave nucleation due to thermal noise. In general, that leads to random spike sequences. The randomness does not arise from small numbers of molecules in the system, but rather from the fact that global events are initiated locally. Stochastic media exhibit almost regular oscillations in the regime of array enhanced coherence resonance (AECR) (10,13–16). Herein wave initiation is frequent enough to ensure that waves emerge as soon as the refractory period has passed. While there is experimental and theoretical evidence for the nucleation of global Ca^{2+} release events by local events (7,9,10), we investigate here whether spike sequences are random.

Transient changes in cytosolic Ca^{2+} concentration are used with great versatility to signal within cells (17). Under appropriate conditions and in many cell types, these transients form oscillations that encompass the entire cell (6,7, 9,17). The interspike interval (ISI) of these oscillations varies from a few seconds to many minutes and their temporal profiles include spikes, sinusoidal oscillations, and bursts (2,3,7).

In many cells, including those examined in this study, oscillatory changes in free cytosolic Ca^{2+} concentration ($[Ca^{2+}]_i$) result from the periodic release of Ca^{2+} from intracellular stores within the endoplasmic reticulum (ER). Release of Ca^{2+} occurs via intracellular Ca^{2+} channels, notably inositol 1,4,5-trisphosphate receptors (IP_3Rs), and Ca^{2+} is then resequestered into the ER by Ca^{2+} pumps (SR/ER Ca^{2+}-ATPases). IP_3Rs are regulated by the Ca^{2+} they conduct, such that fast activation by cytosolic Ca^{2+} and slower inhibition lead to a bell-shaped Ca^{2+}-dependence of the stationary open probability of the IP_3R (18–20). Within the membrane of the ER, clusters of IP_3Rs are separated by perhaps 1–7 μm (8,9,21), and clustering is also dynamically regulated (22,23). These clusters of channels generate global concentration spikes via a hierarchy of Ca^{2+} release events (5–7) that depend upon Ca^{2+} diffusing between IP_3Rs to ignite the activity of successive clusters (3,17). The smallest Ca^{2+} release events, blips (5), probably reflect random openings of single IP_3Rs . Larger events, puffs, lasting tens of milliseconds and restricted to a volume of <0.5 fl, reflect the

Submitted August 9, 2007, and accepted for publication November 9, 2007.

Address reprint requests to Martin Falcke, Tel.: 49-30-80-62-26-27; E-mail: falcke@hmi.de.

Editor: Arthur Sherman.

0006-3495/08/03/2404/08 $2.00

doi: 10.1529/biophysj.107.119495

almost simultaneous opening of a few IP_3Rs within a cluster (5,8,9,21). Many coordinated puffs form oscillations and waves (3,24,25). Ca^{2+} oscillations therefore depend upon both the spatial organization of IP_3Rs and their regulation by Ca^{2+} (19,20,26).

The links between IP_3R behavior and Ca^{2+} oscillations are poorly understood. Is oscillatory behavior a feature of individual IP_3Rs and their local interaction with Ca^{2+} and IP_3, with channels opening and closing in oscillatory fashion? Or do oscillations arise from properties that depend upon a higher level of organization involving many IP_3Rs? Is AECR the new quality added by the more complex organization that would allow oscillations to emerge even from nonoscillatory elements?

With oscillatory dynamics arising from local interactions between individual IP_3Rs and their ligands, each IP_3R cluster is also an oscillator because channels within a cluster are synchronized by Ca^{2+} diffusion (11). Characteristics of the global oscillation, like period and amplitude, would be determined by local parameters such as channel state dynamics. Spatial coupling of channel clusters by Ca^{2+} diffusion would serve only to synchronize the oscillations. The global oscillation is deterministic: it has regular ISI and the timing of each spike is predictable. But recent theoretical studies suggest that IP_3R clusters are not deterministic oscillators (10,27). A deterministic model generates oscillations only if IP_3Rs are exposed to Ca^{2+} concentrations similar to those that cause their half-maximal regulation ($\sim$0.1–10 μM) (18–20,26). Local Ca^{2+} concentrations near open IP_3Rs are much higher, and therefore do not allow for deterministic oscillations (11,27–29).

Another possibility is that stochastic fluctuations render IP_3R clusters oscillatory. Stochastic behavior of IP_3R clusters is observed experimentally as Ca^{2+} puffs (6,9). Simulations show that random binding and dissociation of Ca^{2+} and IP_3 to IP_3Rs are sufficient sources of stochastic fluctuations to explain the random generation of Ca^{2+} puffs (10,30,31). However, these fluctuations alone cannot generate the observed timescale of global oscillations because puff durations and frequencies are 3–100 times faster than the ISI in cells (6). Processes occurring within a single IP_3R cluster do not, therefore, transform random molecular behavior into oscillations. Local processes are not oscillatory, and so the idea that channel clusters are oscillators is untenable. A higher level of spatial organization is required to generate oscillations. The next spatial level is the cell, with its array of IP_3R clusters each capable of generating Ca^{2+} puffs.

That suggests that intracellular Ca^{2+} dynamics behave as a stochastic medium. Experimental and theoretical studies show that Ca^{2+} puffs can initiate global Ca^{2+} spikes (3,6,7,9,10). But theoretical analysis suggests that cells would not then oscillate deterministically; instead, they would produce random sequences of global Ca^{2+} release events (3,10,27,32). In particular, factors that modify spatial coupling would affect both frequency and the ability to oscillate (3,10).

METHODS

Measurements of $[Ca^{2+}]_i$ in glia

Glial cell cultures were prepared from brains of newborn NMRI mice (33) using whole brains for microglia, but only cortex for astrocyte cultures. Cells were loaded with fluo4-AM (5 μM) for 30 min at 20°C in glial medium (148.9 mM NaCl, 5.4 mM KCl, 1 mM $MgCl_2$, 10 mM $CaCl_2$, 5 mM HEPES, and 10 mM D-glucose, at pH 7.4). Cultures were fixed within the microscope chamber by a U-shaped Pt wire and superfused with glial medium at 20°C. Cells were illuminated (495 nm) from a monochromator (TILL Photonics, München, Germany) and fluorescent images (515–545 nm) collected every 3 s with a 12-bit camera (SensiCam, Cooke, Romulus, MI) on an upright microscope and visualized with ImagingCellsEasily software (Max Dulbrück Center, Berlin, Germany).

Measurements of $[Ca^{2+}]_i$ in human embryonic kidney (HEK) cells

HEK293 cells were cultured in Dulbecco's modified Eagle's medium/Ham's F-12 supplemented with fetal bovine serum (10 %) and L-glutamine (2 mM), in a humidified atmosphere (95% air, 5% CO_2, 37°C). Medium was replaced every third day, and cells were passaged when they reached 80% confluence. For single cell imaging, cells were plated onto 22-mm round glass coverslips coated with 0.01% poly-L-lysine and used after two days. They were loaded with 2 μM Fura-2-AM in HEK medium (135 mM NaCl, 5.9 mM KCl, 1.2 mM $MgCl_2$, 1.5 mM $CaCl_2$, 11.6 mM HEPES, 11.5 mM D-glucose, and pH 7.3) supplemented with 1 mg/ml bovine serum albumin and 0.02% Pluronic F-127. Cells were loaded for 45 min at 20°C and then washed for 45 min in HEK medium to allow deesterification of the Fura-2-AM. Measurements of $[Ca^{2+}]_i$ in single cells were performed as previously described (34), with fluorescence collected at intervals of 5 s. Fluorescence ratios were calculated after correction for autofluorescence.

Measurements of $[Ca^{2+}]_i$ in processed lipoaspirate (PLA) cells

The study conforms to the Declaration of Helsinki and all cell donors gave their informed written consent to use part of their fat tissue for the generation of processed lipoaspirate (PLA) cells.

PLA cells were isolated from fat tissue (35) and cultured in 25 cm^2 flasks in 5% CO_2, humidified air at 37°C in Ham's F-10 medium (Biochrom, Berlin, Germany) supplemented with 10% fetal calf serum (Sigma, St. Louis, MO), 2 mM glutamine, 0.1 mM β-mercaptoethanol, 1–100 nonessential amino acids (Biochrom), 100 units/ml penicillin and 100 μg/ml streptomycin (Invitrogen, Carlsbad, CA). Subconfluent cell cultures were dissociated with a 0.2% trypsin-0.05% EDTA solution and subcultured onto 12 mm coverslips. For Ca^{2+} measurements, subconfluent cells on coverslips were incubated for 30 min with 10 μM fluo3-AM (Invitrogen) and then washed once in culture medium. Fluo-3 fluorescence was recorded in single cells by confocal laser-scanning microscopy (laser scanning microscope model No. 510 Meta; Zeiss, Jena, Germany) using a 25$\times$ objective with a numerical aperture of 0.8 (Plan Neofluor; Zeiss). Excitation was at 488 nm and emission was recorded using a 515 nm longpass filter.

DATA ANALYSIS

All fluorescence signals, whether derived from single wavelength or ratiometric indicators, are expressed relative to the baseline fluorescence (ΔF = signal/basal). Because we analyze only interspike intervals (ISIs), there is no need to calibrate ΔF to $[Ca^{2+}]_i$. For each single-cell time series of fluorescence, the time points of the maxima above a minimal level were determined resulting in a series of spike times,

which was used to determine the ISIs. The calculations of statistical characteristics require a stationary ISI series. However, most experimental records of HEK cells have a slight trend and eventually stop oscillating. We reduced that trend by leaving out parts of the ISI series in the beginning and end showing very obvious trends and removed linear trend from the remaining series before we calculated the average period T_{av}, the standard deviation σ, and correlations. This is illustrated in Supplementary Material Fig. S7.

Correlation coefficients ρ_k between an ISI and its k^{th} successor for the l^{th} ISI-series were calculated according to

$$\rho_k^{(l)} = \left\langle \frac{\mathrm{Cov}(ISI_i^{(l)}, ISI_{i+k}^{(l)})}{\sigma_i^{(l)}\sigma_{i+k}^{(l)}} \right\rangle_i. \quad (1)$$

With the $\rho_k^{(l)}$, we formed the population average across n cells by $\rho_k = (1/n)\sum_{l=1}^{n}\rho_k^{(l)}$.

T_{av}-σ relation for time-dependent global nucleation rate

We show that a global nucleation probability increasing by a relaxation to an asymptotic value provides T_{av}-σ relations compatible with our findings. We choose a time-dependent nucleation rate Λ like

$$\Lambda(t) = \lambda(1 - e^{-\xi t}), \quad (2)$$

with the regeneration rate ξ. The value ξ could describe, e.g., the recovery from inhibition (36). The probability of observing a global wave at time t is given by

$$p(t) = \lambda(1 - e^{-\xi t})\exp\left[-\int_0^t \lambda(1 - e^{-\xi t'})dt'\right]. \quad (3)$$

With this expression we can calculate the first two moments as

$$T_{av} = \int_0^\infty t\lambda(1 - e^{-\xi t})\exp\left[-\int_0^t \lambda(1 - e^{-\xi t'})dt'\right]dt, \quad (4)$$

$$\langle T^2\rangle = \int_0^\infty t^2\lambda(1 - e^{-\xi t})\exp\left[-\int_0^t \lambda(1 - e^{-\xi t'})dt'\right]dt. \quad (5)$$

That can be integrated by parts,

$$T_{av} = \int_0^\infty te^{-f(t)}f'(t)dt = -te^{-f(t)}|_0^\infty + \int_0^\infty e^{-f(t)}dt, \quad (6)$$

where the first term vanishes, leading to

$$T_{av} = \int_0^\infty e^{-\lambda\left(t + \frac{1}{\xi}e^{-\xi t} - \frac{1}{\xi}\right)}dt \quad (7)$$

for T_{av}. $\langle T^2\rangle$ is given by

$$\langle T^2\rangle = \int_0^\infty t^2e^{-f(t)}f'(t)dt = 2\int_0^\infty te^{-f(t)}dt = 2\int_0^\infty te^{-\lambda\left(t + \frac{1}{\xi}e^{-\xi t} - \frac{1}{\xi}\right)}dt. \quad (8)$$

Integration yields

$$T_{av} = \frac{e^{\frac{\lambda}{\xi}}\left(\frac{\lambda}{\xi}\right)^{1-\frac{\lambda}{\xi}}}{\lambda}\left[\Gamma\left(\frac{\lambda}{\xi}\right) - \Gamma\left(\frac{\lambda}{\xi}, \frac{\lambda}{\xi}\right)\right], \quad (9)$$

$$\langle T^2\rangle = \frac{2e^{\frac{\lambda}{\xi}}}{\lambda^2}\mathcal{F}\left[\left(\frac{\lambda}{\xi}, \frac{\lambda}{\xi}\right), \left(1 + \frac{\lambda}{\xi}, 1 + \frac{\lambda}{\xi}\right), -\frac{\lambda}{\xi}\right], \quad (10)$$

where $\Gamma(x)$ denotes the Euler Γ-function, $\Gamma(x, y)$ the incomplete γ-function, and F[**x**] is the generalized hypergeometric function ${}_2F_2(\mathbf{x})$. With the relation for the standard deviation

$$\sigma = \sqrt{\langle T^2\rangle - T_{av}^2}, \quad (11)$$

we obtain the T_{av}-σ relations shown in Fig. 1.

We did not consider a deterministic part T_d of the ISI in the above calculations, which represents an absolute refractory part of the ISI. Such a deterministic part simply moves the curves in Fig. 1 to larger values of T_{av}. The complete distribution including T_d is

$$p(t) = \begin{cases} 0, & t < T_d \\ \lambda(1 - e^{-\xi(t - T_d)})\exp\left[-\int_{T_d}^t \lambda(1 - e^{-\xi(t' - T_d)})dt'\right], & t \geq T_d \end{cases}. \quad (12)$$

The analysis of experimental data showed that T_{av}, σ, and T_d vary between individual cells of the same cell type.

RESULTS AND DISCUSSION

To establish whether intracellular Ca^{2+} oscillations are deterministic or stochastic, we performed comprehensive measurements of ISI series in different cell types. In each case, IP_3Rs evoke the Ca^{2+} oscillations (37–39) (Fig. S8). Fig. 2 shows representative time series of global oscillations in astrocytes, microglia, PLA stem cells from human adipose

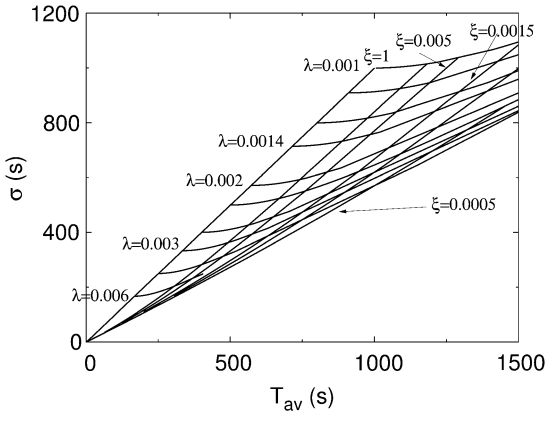

FIGURE 1 T_{av}-σ relation resulting from Eqs. 7 and 8. The lines ξ = *constant* arise by varying λ. They start at (0,0) with $\lambda = \infty$ and converge to $T_{av} = \sigma$ with increasing ξ. The lines λ = *constant* start on $T_{av} = \sigma = \lambda^{-1}$ with $\xi \gg \lambda$ very large. Note that the T_{av}-σ relation becomes linear for $\lambda/\xi \to 0$ or $T_{av} \to \infty$ and $\sigma \to \infty$ and that the slope decreases from one for $\xi \to 0$. The values ξ and λ are measured in s^{-1}.

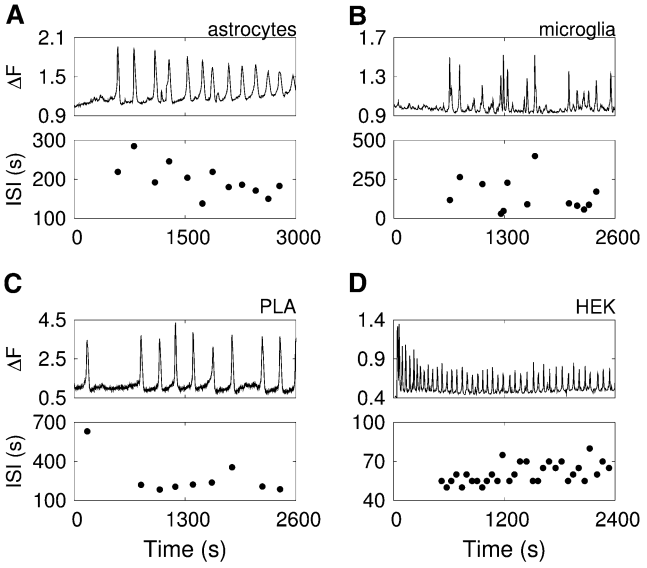

FIGURE 2 IP_3-mediated Ca^{2+} spikes in diverse cells. Representative examples of oscillation time series for astrocytes (*A*), microglia (*B*), PLA cells (*C*), and HEK cells stimulated with 30 μM carbamyl choline (CCh) (*D*). The oscillations in panels *A–C* are spontaneous. Changes in the fluorescence of the Ca^{2+} indicator relative to its basal level (ΔF) report the increase in free cytosolic [Ca^{2+}]. Lower panels show the ISI after each spike, with ISI defined as the interval between consecutive fluorescence maxima.

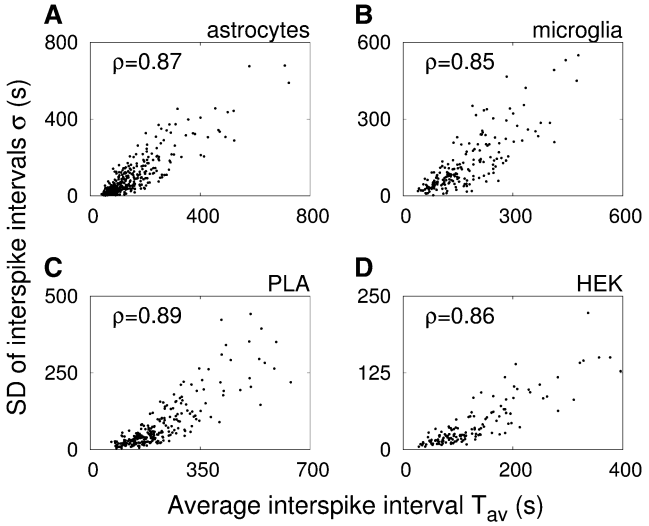

FIGURE 3 Ca^{2+} spikes occur randomly. Dependence of the standard deviation σ of ISI on the average ISI T_{av} for 366 astrocytes (*A*), 224 microglia (*B*), 270 PLA cells (*C*), and 137 HEK cells stimulated with 30 μM CCh (*D*). σ and T_{av} were obtained from time series of single cells by temporal averaging. The correlation coefficient ρ shows that σ and T_{av} are highly correlated in all four cases.

tissue, and human embryonic kidney (HEK) cells. These examples show that ISIs are not regular. The length of the ISI changes randomly. Records like these were used to determine the serial correlation coefficients ρ_k, mean values T_{av}, and standard deviations σ of ISI. For all cell types and with all degrees of stimulation, σ increases with T_{av} (Fig. 3).

Standard deviations are of the same order of magnitude as averages for most points, and for large T_{av}, σ and T_{av} are similar. Hence, the uncertainty in predicting the occurrence of a spike is of the same order as the mean ISI: i.e., Ca^{2+} spikes are random events. If spikes represented the active phase in a deterministic oscillation, the standard deviation of ISI would instead be in the range of the global interpuff interval, i.e., between a few hundred milliseconds for short T_{av} and a few seconds for long T_{av}. The uncertainty in spike timing shows in the correlation coefficients ρ_k of the ISI time series between the i^{th} and $(i + k)^{th}$ ISI (Fig. 4). Consecutive intervals are not correlated, confirming the randomness of the spike-generating mechanism.

We conclude that global oscillations result from a sequence of randomly occurring global Ca^{2+} spikes. The data show also that σ almost vanishes at the smallest values of T_{av}, indicating that almost regular oscillations with ISIs close to T_d do exist. The results are similar for spontaneous oscillations in astrocytes, microglia, and PLA cells, and for oscillations evoked by different levels of stimulation in HEK cells, suggesting that IP_3-evoked Ca^{2+} oscillations are sequences of stochastic spikes in many cell types.

Our conclusion is compatible with the idea that each Ca^{2+} spike reflects the passage of a Ca^{2+} wave across the cell driven by successive activation of IP_3R clusters by Ca^{2+} diffusing between them (6,7,9). This mechanism can generate the spectrum of observed shapes of oscillations (3,10). Our results show that waves initiate randomly. The time of initiation is not set by a deterministic process, such as recovery from Ca^{2+}-inhibition or a progressive sensitization of IP_3Rs by Ca^{2+}.

Stochastic models of repetitive waves show that if σ is of the same order as T_{av}, it is dominated by the probability (P_{trig}) of triggering a wave after the cell has recovered from the previous one (10). The smaller the value of P_{trig}, the longer it takes on average for the next wave to occur, and the larger is the value of σ. For such repetitive triggering of waves, σ increases linearly with T_{av}, and $\sigma = 1/P_{trig}$ holds for large values of T_{av}. Even if P_{trig} relaxes exponentially from 0 immediately after a spike to an asymptote, the linear relation between σ and T_{av} for large T_{av} still holds and it has a slope <1 (see Fig. 1 and Fig. 3 *D*). Such a relaxation of P_{trig} appears to apply also to wave initiation reported in Marchant and Parker (9). Almost regular oscillations arise when P_{trig} is very large, because then as soon as the cell has recovered from one spike, the next one is triggered. We refer to the length of the ISI of these regular oscillations as the deterministic part T_d of the ISI. It might be set by a variety of processes depending on cell type, for example: store refilling, IP_3R inhibition, or Ca^{2+}-feedback to the IP_3 concentration. Each of these processes may also cause a time-dependence of P_{trig} such as that described in a simplified way by the relaxation with time constant ξ in Eq. 2.

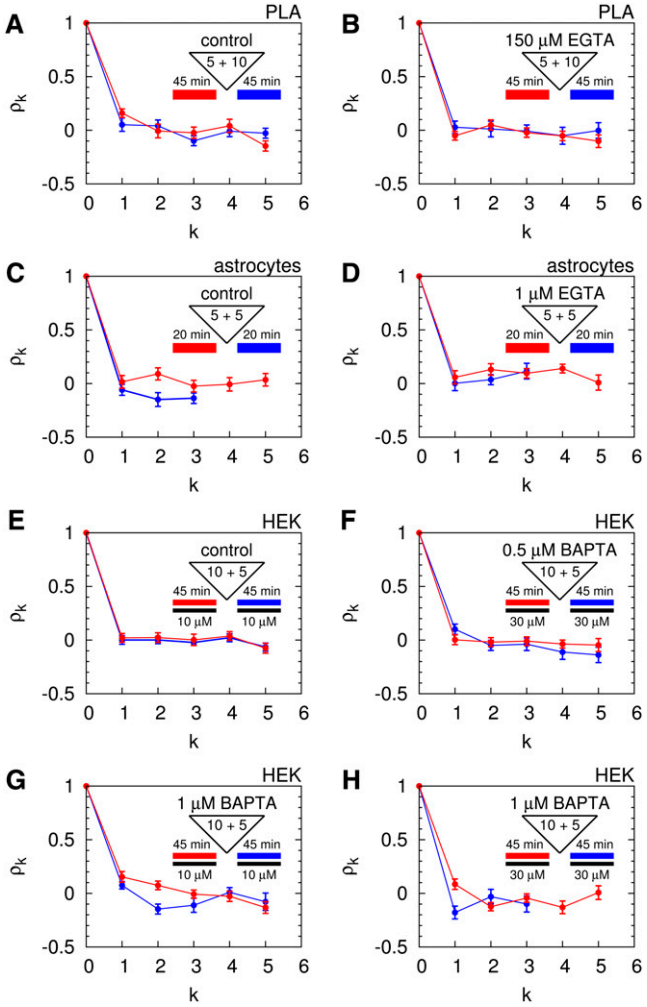

FIGURE 4 Successive ISI are not correlated. Correlation coefficient ρ_k between the i^{th} and $(i+k)^{th}$ ISI averaged across n time series obtained in the experiments shown in Fig. 6 before (*red*) and after (*blue*) loading with additional Ca^{2+} buffer. The protocols are shown in the insets (see also caption of Fig. 6). The number of time series measured for the first and the second periods were, respectively: (*A*) $n_1 = 27$, $n_2 = 20$; (*B*) $n_1 = 35$, $n_2 = 18$; (*C*) $n_1 = 36$, $n_2 = 35$; (*D*) $n_1 = 33$, $n_2 = 23$; (*E*) $n_1 = 35$, $n_2 = 35$; (*F*) $n_1 = 35$, $n_2 = 28$; (*G*) $n_1 = 31$, $n_2 = 22$; and (*H*) $n_1 = 29$, $n_2 = 18$. Error bars show standard error for averaging over n time series.

The time-dependence of the global nucleation rate differs between the different cell types as revealed by the slopes of the relationship between σ and T_{av}. Fig. 5 shows values of the parameters of the time-dependent global nucleation rate (Eq. 2) for the different cell types. The spontaneous oscillations in astrocytes and microglia have a slope of the σ-T_{av}-relation close to 1 and an asymptotic nucleation rate λ much smaller than the relaxation rate ξ. Despite the relatively fast recovery from the previous spike, these oscillations are neither fast nor regular, since the asymptotic nucleation rate λ of these cells is small. The stimulated oscillations in HEK cells show the inverse relation between λ and ξ. That is correlated with the information content of stimulated and spontaneous oscillations which increases with increasing λ/ξ (40).

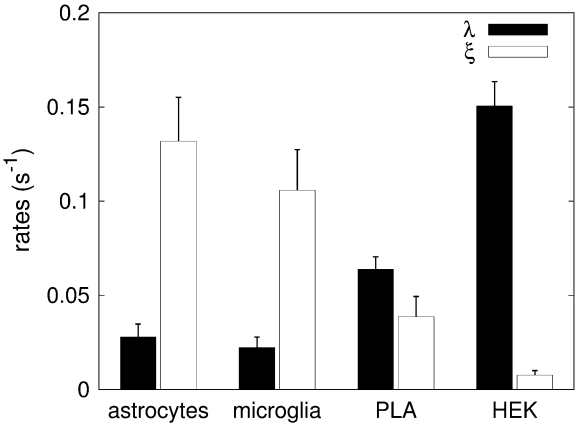

FIGURE 5 Values of the parameters λ and ξ of the time-dependent global nucleation rate Eq. 2 for the different cell types. The values were obtained by fitting σ and T_{av} of individual time series to Eqs. 10 and 11 to obtain λ and ξ, which were then averaged across all cells of the same type. We have approximated T_d by the smallest value of T_{av} observed for the corresponding cell type in the fitting procedure. Error bars show standard error.

Recovery from the previous spike is relatively slow in HEK cells. That corresponds to the initial decline in spike amplitudes in Fig. 2 during which the cell reaches a state corresponding to incomplete recovery from a spike during each ISI. One possibility is that insufficient refilling of the ER causes the decline. We might then suggest that immediately after stimulation, Ca^{2+} reuptake during the ISI fails to keep pace with release during a spike and successive Ca^{2+} transients decrease in amplitude. But during the stationary phase of oscillations, the two fluxes come into balance such that Ca^{2+} uptake by the stores during the ISI matches the amount released during the preceding spike. The time-dependent nucleation rate $\Lambda(t)$ reaches only 60% of λ during an average ISI due to the small value of ξ. However, since the asymptotic nucleation rate λ is rather large, the oscillations in HEK cells have smaller σ than astrocyte oscillations. The values for λ and ξ of PLA cells lie between those for astrocytes and HEK cells.

We can further examine the stochastic component of wave triggering by manipulating the probability of wave initiation, for example by increasing the Ca^{2+}-buffering capacity of the cytosol (10,11). Decreasing P_{trig} increases the average ISI, but if wave triggering is random, the standard deviation σ should also increase. P_{trig} is actually the probability of two sequential events: that a puff occurs (P_{puff}) and then that the puff ignites a wave (P_{wave}). The latter turns the puff frequency into the smaller wave frequency ($P_{trig} = P_{puff}P_{wave}$) and the standard deviation of interpuff intervals into the standard deviation of interspike intervals. P_{wave} is expected to decrease when diffusion of free Ca^{2+} between clusters (the spatial coupling) is reduced by buffers (11). The precise effect depends on the dynamic regime of the cell. With slow irregular waves, a slight decrease in coupling is predicted to increase T_{av} and σ, while larger decreases are predicted to abolish the

self-amplifying mechanism required for oscillations leaving only moderate puff activity (10,11). Oscillations are predicted to be very sensitive to addition of Ca^{2+} buffers with fast binding and dissociation rates, and with K_d^{Ca} similar to resting cytosolic Ca^{2+} concentration because such buffers effectively reduce diffusion of free Ca^{2+} at distances similar to the likely spacings of IP_3R clusters (11). Because the buffers we use do not change the resting cytosolic free Ca^{2+} concentration, the IP_3 concentration, or the interactions between IP_3Rs within clusters (41), we do not expect them to affect P_{puff}.

We measured the effect of Ca^{2+}-buffering on oscillations in astrocytes, HEK cells, and PLA cells. Oscillations were first recorded to establish T_{av} and σ. The buffering capacity of the cells was then increased by incubating the cells with BAPTA-AM or EGTA-AM, before continuing measurements of $[Ca^{2+}]_i$. BAPTA loading caused most of the HEK cells to stop oscillating, and for the cells that resumed oscillations (~50% for cells loaded with 0.5 or 1 M BAPTA-AM), T_{av} and σ were both increased in a concentration-dependent way (Fig. 6, *D–F*). EGTA loading of PLA cells and astrocytes also caused oscillations to terminate in ~80% of cells, and increased both T_{av} and σ in the cells that resumed oscillations (Fig. 6, *A–C*, *G–I*).

The results demonstrate both the exquisite sensitivity of Ca^{2+} oscillations to Ca^{2+} buffering, whether provided by fast (BAPTA) or slow (EGTA) Ca^{2+} buffers, and the increase in both T_{av} and σ predicted for a stochastic mechanism dependent on repetitive Ca^{2+} waves (10).

We have shown that cells use a stochastic mechanism to generate global Ca^{2+} spikes. With ~10^4 IP_3Rs in each HEK cell (unpublished) and far more Ca^{2+} ions, why does random behavior play such an important part in Ca^{2+} spiking? The reason is that, as for any stochastic medium, global events are initiated by local processes. A puff changes the local free Ca^{2+} concentration by 100–1000-fold (11) and the gradients are so steep that only neighboring IP_3R clusters experience the change. Each puff, occurring within only a small part of the cell, is a potential wave initiation site, and the few IP_3R clusters that participate in the initiation of each wave are too few for the process to become deterministic. These properties identify intracellular Ca^{2+} dynamics as a random medium. The existence of so-called hot-spots (5) does not change these

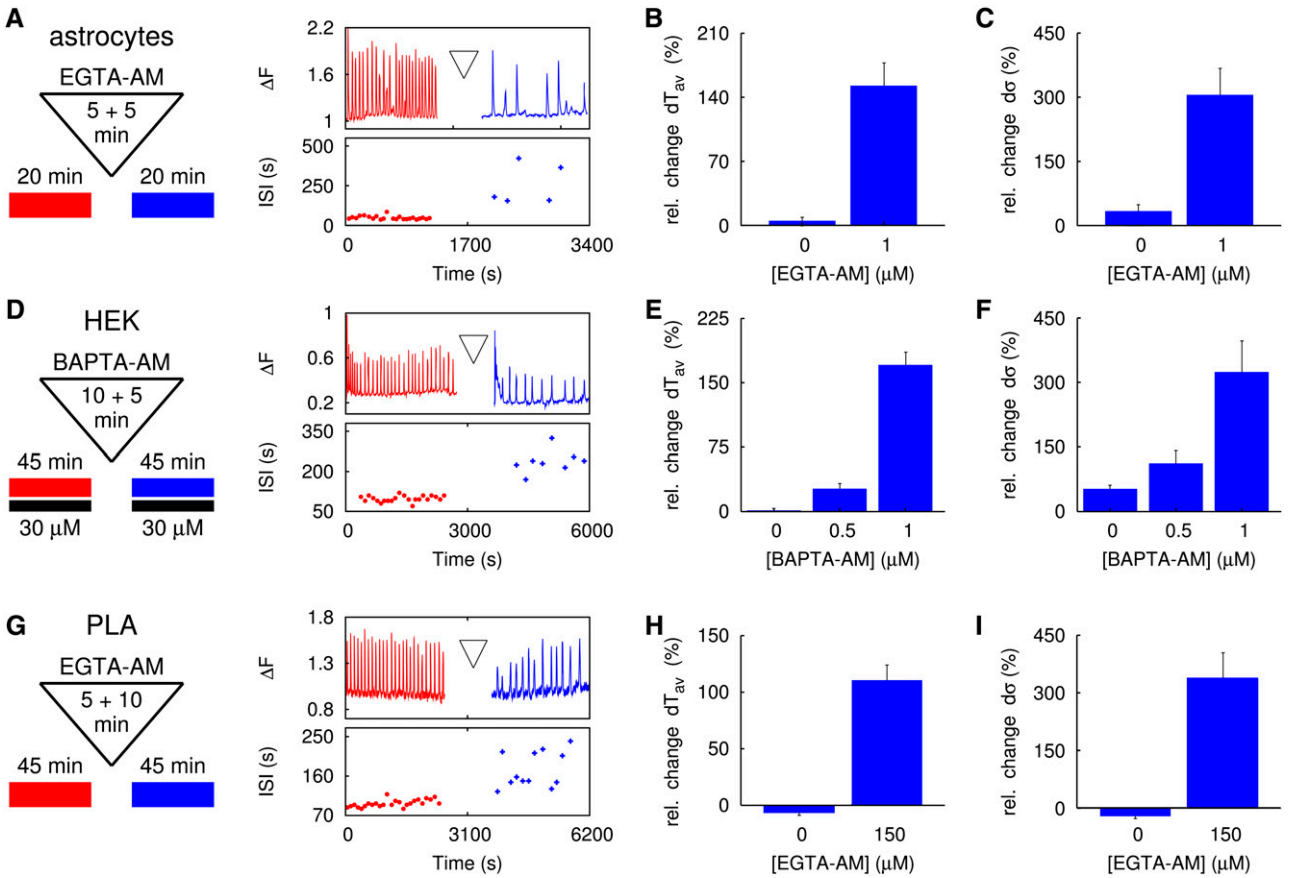

FIGURE 6 Ca^{2+} buffers render spike times even less predictable. Results show Ca^{2+} spikes in astrocytes (*A–C*), HEK cells stimulated with 30 μM CCh (*D–F*), and PLA cells (*G–I*) before (*red*) and after (*blue*) loading with additional Ca^{2+} buffer. The protocols and typical results are shown in panels *A*, *D*, and *G*; the durations of the loading and subsequent hydrolysis times are shown in the triangles. Changes to concentrations of EGTA-AM or BAPTA-AM are shown in the histograms. For the 50% of cells that resumed Ca^{2+} spiking, changes dT_{av} and $d\sigma$ in T_{av} and σ are shown relative to the values obtained before incubation with the Ca^{2+} buffer. Error bars show standard error from different cells and experiments.

conclusions; it simply means that P_{puff} is not spatially homogeneous.

Intracellular Ca^{2+} spikes occur randomly. But a regular regime exists if P_{trig} is high due to the existence of a deterministic part of the ISI. The mean and the standard deviation of the ISI distribution depend on spatial coupling. The regular Ca^{2+} spikes are thus an example of array enhanced coherence resonance, an intrinsically stochastic phenomenon (10,13, 15,16,42). This is consistent with hierarchical recruitment of Ca^{2+} release events (6,7). Hence, oscillations are an emergent property of arrays of IP_3R clusters and not a property of single IP_3Rs. Ca^{2+} oscillations are the first example of the constructive use of noise in cell signaling and the first experimental verification of AECR in a natural system.

These conclusions are based on the data presented here, previous measurements on the initiation of spikes and waves (6,7,9,43) and on theoretical studies investigating the role of noise and spatial coupling for global signals (10,16,42,44, 45). It is accepted that elemental events like Ca^{2+} puffs and sparks are random (3,30,31,46–53), but this has not previously been shown for global events. Indeed, and despite the observation that over a large area of the cytosol (8 μm $\times$ 8 μm) of a *Xenopus* oocyte σ increases with T_{av} (9), it has been assumed that global signals are deterministic (2).

The probability of initiating a wave (P_{trig}) is determined by local properties, such as channel state dynamics, numbers of channels in a cluster, release currents, and by diffusion of free Ca^{2+} between clusters. P_{trig} sets σ of the ISI distribution. Information on local properties, like the open probability in vivo, can thus, in principle, be obtained from the fluctuations of the global Ca^{2+} signal.

We have shown that in many different cell types IP_3-evoked Ca^{2+} spikes are caused by random wave nucleation with a regular regime arising from AECR. The randomness of spike trains does not prevent Ca^{2+} oscillations from transmitting information. As long as the ISI distribution of stimulated spike trains is sufficiently different from the ISI distribution of spontaneous spiking (40), cells can distinguish the message from the noise.

SUPPLEMENTARY MATERIAL

To view all of the supplemental files associated with this article, visit www.biophysj.org.

A.S. is supported by the International Research Training Group of the Deutschen Forschungsgemeinschaft (grant No. GRK 1360). C.W.T. and S.C.T. are supported by the Wellcome Trust.

REFERENCES

1. van Kampen, N. G. 2001. Stochastic Processes in Physics and Chemistry. North-Holland, Amsterdam, The Netherlands.
2. Schuster, S., M. Marhl, and T. Höfer. 2001. Modeling of simple and complex calcium oscillations. *Eur. J. Biochem.* 269:1333–1355.
3. Falcke, M. 2004. Reading the patterns in living cells—the physics of Ca^{2+} signaling. *Adv. Phys.* 53:255–440.
4. Goldbeter, A. 1996. Biochemical Oscillations and Cellular Rhythms. Cambridge University Press, Cambridge, UK.
5. Parker, I., J. Choi, and Y. Yao. 1996. Elementary events of $InsP_3$-induced Ca^{2+} liberation in *Xenopus* oocytes: hot spots, puffs and blips. *Cell Calcium.* 20:105–121.
6. Marchant, J., N. Callamaras, and I. Parker. 1999. Initiation of IP_3-mediated Ca^{2+} waves in *Xenopus* oocytes. *EMBO J.* 18:5285–5299.
7. Bootman, M. D., M. Berridge, and P. Lipp. 1997. Cooking with calcium: the recipes for composing global signals from elementary events. *Cell.* 91:367–373.
8. Thomas, D., P. Lipp, M. Berridge, and M. D. Bootman. 1998. Hormone-evoked elementary Ca^{2+} signals are not stereotypic, but reflect activation of different size channel clusters and variable recruitment of channels within a cluster. *J. Biol. Chem.* 273:27130–27136.
9. Marchant, J., and I. Parker. 2001. Role of elementary Ca^{2+} puffs in generating repetitive Ca^{2+} oscillations. *EMBO J.* 20:65–76.
10. Falcke, M. 2003. On the role of stochastic channel behavior in intracellular Ca^{2+} dynamics. *Biophys. J.* 84:42–56.
11. Thul, R., and M. Falcke. 2004. Release currents of IP_3 receptor channel clusters and concentration profiles. *Biophys. J.* 86:2660–2673.
12. Zaccolo, M., and T. Pozzan. 2002. Discrete microdomains with high concentration of cAMP in stimulated rat neonatal cardiac myocytes. *Science.* 295:1711–1715.
13. Pikovsky, A. S., and J. Kurths. 1997. Coherence resonance in a noise-driven excitable system. *Phys. Rev. Lett.* 78:775–778.
14. Jung, P., and G. Mayer-Kress. 1995. Spatiotemporal stochastic resonance in excitable media. *Phys. Rev. Lett.* 74:2130–2133.
15. Lindner, B., J. Garcia-Ojalvo, A. Neimann, and L. Schimansky-Geier. 2004. Effects of noise in excitable systems. *Phys. Rep.* 392:321–424.
16. Coombes, S., and Y. Timofeeva. 2003. Sparks and waves in a stochastic fire-diffuse-fire model of Ca^{2+} release. *Phys. Rev. E Stat. Nonlin. Soft Matter Phys.* 68:021915.
17. Berridge, M. J., P. Lipp, and M. D. Bootman. 2000. The versatility and universality of calcium signaling. *Nat. Rev. Mol. Cell Biol.* 1:11–22.
18. Bezprozvanny, I., J. Watras, and B. E. Ehrlich. 1991. Bell-shaped calcium-response curves of $Ins(1,4,5)P_3$- and calcium-gated channels from endoplasmic reticulum of cerebellum. *Nature.* 351:751–754.
19. Taylor, C. W., and A. Laude. 2002. IP_3 receptors and their regulation by calmodulin and cytosolic Ca^{2+}. *Cell Calcium.* 32:321–334.
20. Mak, D., S. McBride, and J. Foskett. 1998. Inositol 1,4,5-tris-phosphate activation of inositol tris-phosphate receptor Ca^{2+} channel by ligand tuning of Ca^{2+} inhibition. *Proc. Natl. Acad. Sci. USA.* 95: 15821–15825.
21. Suhara, W., M. Kobayashi, H. Sagara, K. Hamadad, T. Goto, I. Fujimoto, K. Torimitsu, and K. Mikoshiba. 2006. Visualization of inositol 1,4, 5-trisphosphate receptor by atomic force microscopy. *Neurosci. Lett.* 391:102–107.
22. Tateishi, Y., M. Hattori, T. Nakayama, M. Iwai, H. Bannai, T. Nakamura, T. Michikawa, T. Inoue, and K. Mikoshiba. 2004. Cluster formation of inositol 1,4,5-trisphosphate receptor requires its transition to open state. *J. Biol. Chem.* 280:6816–6822.
23. Chalmers, M., M. J. Schell, and P. Thorn. 2006. Agonist-evoked inositol trisphosphate receptor (IP_3R) clustering is not dependent on changes in the structure of the endoplasmic reticulum. *Biochem. J.* 394:57–66.
24. Rooney, T. A., S. K. Joseph, C. Queen, and A. P. Thomas. 1996. Cyclic GMP induces oscillatory calcium signals in rat hepatocytes. *J. Biol. Chem.* 271:19817–19825.
25. Charles, A. C., E. R. Dirksen, J. E. Merrill, and M. J. Sanderson. 1991. Intercellular signaling in glial cells: calcium waves and oscillations in response to mechanical stimulation and glutamate. *Neuron.* 6:983–992.
26. Adkins, C. E., and C. W. Taylor. 1999. Lateral inhibition of inositol 1,4, 5-trisphosphate receptors by cytosolic Ca^{2+}. *Curr. Biol.* 9:1115–1118.
27. Thul, R., and M. Falcke, 2004. Stability of membrane-bound reactions. *Phys. Rev. Lett.* 93:188103-1–4.

28. Shuai, J., H. J. Rose, and I. Parker. 2006. The number and spatial distribution of IP_3 receptors underlying calcium puffs in *Xenopus* oocytes. *Biophys. J.* 91:4033–4044.

29. Bentele, K., and M. Falcke. 2007. Quasi-steady approximation for ion channel currents. *Biophys. J.* In press. 10.1529/biophysj.107.104299.

30. Swillens, S., G. Dupont, and P. Champeil. 1999. From calcium blips to calcium puffs: theoretical analysis of the requirements for interchannel communication. *Proc. Natl. Acad. Sci. USA.* 96:13750–13755.

31. Shuai, J., and P. Jung. 2002. Stochastic properties of Ca^{2+} release of inositol 1,4,5-trisphosphate receptor clusters. *Biophys. J.* 83:87–97.

32. Thul, R., and M. Falcke. 2006. Frequency of elemental events of intracellular Ca^{2+} dynamics. *Phys. Rev. E Stat. Nonlin. Soft Matter Phys.* 73:061923.

33. Lyon, S., and H. Kettenmann. 1998. Oligodendrocytes and microglia are selectively vulnerable to combined hypoxia and hypoglycemia injury in vitro. *J. Cereb. Blood Flow Metab.* 18:521–530.

34. Short, A. D., and C. W. Taylor. 2000. Parathyroid hormone controls the size of the intracellular Ca^{2+} stores available to receptors linked to inositol trisphosphate formation. *J. Biol. Chem.* 275:1807–1813.

35. Zuk, P. A., M. Zhu, P. Ashjian, D. A. De Ugarte, J. I. Huang, H. Mizuno, Z. C. Alfonso, J. K. Fraser, P. Benhaim, and M. H. Hedrick. 2002. Human adipose tissue is a source of multipotent stem cells. *Mol. Biol. Cell.* 13:4279–4295.

36. Falcke, M. 2004. Period distributions of intracellular Ca^{2+} oscillations. Proceedings of the Fourth International Workshop on Bioinformatics and Systems Biology, May 31-June 3, 2004, Kyoto, Japan. Short papers: IBSB 2004. Poster Abstracts: 5–6.

37. Fiacco, T. A., and K. D. McCarthy. 2006. Astrocyte calcium elevations: properties, propagation, and effects on brain signaling. *Glia.* 54:676–690.

38. Färber, K., and H. Kettenmann. 2006. Functional role of calcium signals for microglial function. *Glia.* 54:656–665.

39. Short, A. D., G. Winston, and C. W. Taylor. 2000. Different receptors use inositol trisphosphate to mobilize Ca^{2+} from different intracellular pools. *Biochem. J.* 351:683–686.

40. Skupin, A., and M. Falcke. 2008. Statistical properties and information content of calcium oscillations. *Genome Inform.* 18.

41. Dargan, S., and I. Parker. 2003. Buffer kinetics shape the spatiotemporal patterns of IP_3-evoked Ca^{2+} signals. *J. Physiol.* 553:775–788.

42. Shuai, J., and P. Jung. 2003. Optimal ion channel clustering for intracellular calcium signaling. *Proc. Natl. Acad. Sci. USA.* 100:506–510.

43. Dupont, G., S. Swillens, C. Clair, T. Tordjmann, and L. Combettes. 2000. Hierarchical organization of calcium signals in hepatocytes: from experiments to models. *Biochim. Biophys. Acta.* 1498:134–152.

44. Falcke, M. 2003. Buffers and oscillations in intracellular Ca^{2+} dynamics. *Biophys. J.* 84:28–41.

45. Falcke, M. 2003. Building a wave—models of the puff-to-wave transition. *In* Understanding Calcium Dynamics: Experiments and Theory. Springer, New York, NY.

46. Parker, I., and Y. Yao. 1995. Calcium puffs in *Xenopus* oocytes. *In* Calcium Waves, Gradients and Oscillations, Ciba F. Symposium. Wiley, Chichester, England.

47. Yao, Y., and I. Parker. 1995. Quantal puffs of intracellular Ca^{2+} evoked by inositol trisphosphate in *Xenopus* oocytes. *J. Physiol.* 482:533–553.

48. Lipp, P., D. Thomas, M. Berridge, and M. Bootman. 1997. Nuclear calcium signaling by individual cytoplasmic calcium puffs. *EMBO J.* 16:7166–7173.

49. Heemskerk, J., G. Willems, M. Rook, and S. Sage. 2001. Ragged spiking of free calcium in ADP-stimulated human platelets: regulation of puff-like calcium signals in vitro and ex vivo. *J. Physiol.* 535: 625–635.

50. Cheng, H., W. Lederer, and M. Cannel. 1993. Calcium-sparks: elementary events underlying excitation-contraction coupling in heart muscle. *Science.* 262:740–744.

51. Smith, G., J. Keizer, M. Stern, W. Lederer, and H. Cheng. 1998. A simple numerical model of calcium spark formation and detection in cardiac myocytes. *Biophys. J.* 75:15–32.

52. Lukyanenko, V., and S. Györke. 1999. Ca^{2+} sparks and Ca^{2+} waves in saponin-permeabilized rat ventricular myocytes. *J. Physiol.* 521: 575–585.

53. Rengifo, J., R. Rosales, A. González, H. Cheng, M. Stern, and E. Ríos. 2002. Intracellular Ca^{2+} release as irreversible Markov process. *Biophys. J.* 83:2511–2521.